



“One tube killing two birds”: Simultaneously boosting the separation and mechanical performances of block copolymer membranes by sparsely doping carbon nanotubes

Xiang Ying^a, Shoutian Qiu^{b,c,**}, Zhuo Li^a, Lei Wang^a, Kang Zhou^a, Xiangyue Ye^a, Jiemei Zhou^a, Sheng Cui^{b,c}, Yong Wang^{a,d,*} 

^a State Key Laboratory of Materials-Oriented Chemical Engineering, College of Chemical Engineering, Nanjing Tech University, Nanjing, 211816, Jiangsu, PR China

^b College of Materials Science and Engineering, State Key Laboratory of Materials-Oriented Chemical Engineering, Nanjing Tech University, Nanjing, 211816, Jiangsu, PR China

^c Jiangsu Collaborative Innovation Center for Advanced Inorganic Function Composites, Nanjing, 211816, Jiangsu, PR China

^d School of Energy and Environment, Southeast University, Nanjing, 210096, Jiangsu, PR China

ARTICLE INFO

Keywords:

Block copolymers
Carbon nanotubes
Melt spinning
Selective swelling
Hollow-fiber membranes

ABSTRACT

Selective swelling of block copolymers as an emerging process to prepare ultrafiltration membranes is receiving growing interests. Herein, we report that very little dosages of carbon nanotubes (CNTs) are able to significantly enhance both the separation and mechanical performances of melt-spun polysulfone-*block*-poly(ethylene glycol) (PSF-*b*-PEG) hollow-fiber membranes. CNTs are adequately dispersed in the block copolymer by melt processing, and exhibit π - π interaction to the PSF continuous phase but repulsion to the PEG dispersed phase. The incompatibility between CNTs and PEG leads to interfacial gaps between CNTs and the PEG phase, thus providing another set of pores facilitating water permeance. Both dosages and aspects of CNTs significantly influence the pore structure and performances of the membranes. Higher dosages of CNTs produce more interfacial gaps and lead to increased porosity and permeance. While CNTs with lower aspects tend to be distributed in the PSF phase, thus producing smaller pores and decreasing permeance by refraining selective swelling to a larger degree. The hollow-fiber membrane doped with 0.01 wt% CNTs having a diameter of \sim 10–20 nm and a length of \sim 50 μ m shows a water permeance increased by three times and a rejection increased by 1.6 times. Moreover, thus-doped membrane exhibits over 1.5 times increase both in tensile stress and the strain at break and multiple times increase in swing tolerance. Such an extremely low dosage of CNTs synchronously boosting membrane permeance, rejection, and mechanical properties is highly desired in practical applications and is expected to be extended in the performance-upgrading of other membranes with multiphases.

1. Introduction

Selective swelling of block copolymers (BCPs), an emerging pore-making strategy, is receiving growing interests because of its extremely facile and efficient features [1,2]. Based on the difference in affinity of the constituent blocks of the microphase-separated BCPs to the swelling agent, well-defined porous structures with pore sizes within the range of \sim 5–50 nm are readily formed [3]. Thus-obtained nanoporous BCPs exhibit strong inherent surface hydrophilicity or

hydrophobicity due to the surface enrichment of the minority blocks during selective swelling, and have been promisingly used in ultrafiltration [4], hemodialysis [5], membrane distillation [6] and lithium-ion battery separators [7].

Hollow-fiber membranes (HFMs), with the typical self-supporting nature and large specific surface areas owing to their hollow cylindrical geometry, usually exhibit good flexibility and excellent mechanical strengths [8,9]. Recently, hollow-fiber membranes prepared by selective swelling of polysulfone-*block*-poly(ethylene glycol) (PSF-*b*-PEG) were

* Corresponding author. State Key Laboratory of Materials-Oriented Chemical Engineering, College of Chemical Engineering, Nanjing Tech University, Nanjing, 211816, Jiangsu, PR China.

** Corresponding author. College of Materials Science and Engineering, State Key Laboratory of Materials-Oriented Chemical Engineering, Nanjing Tech University, Nanjing, 211816, Jiangsu, PR China.

E-mail addresses: qiust@njtech.edu.cn (S. Qiu), yongwang@seu.edu.cn (Y. Wang).

<https://doi.org/10.1016/j.memsci.2025.124019>

Received 22 December 2024; Received in revised form 15 March 2025; Accepted 22 March 2025

Available online 22 March 2025

0376-7388/© 2025 Elsevier B.V. All rights reserved, including those for text and data mining, AI training, and similar technologies.

reported to be good candidates in applications such as protein separations and hemodialysis [10]. However, the permeances of membranes by selective swelling are moderate due to their symmetrical structure and relatively thick wall thickness of thus-prepared membranes [3]. Furthermore, hollow-fiber membranes with larger diameters and higher pore volumes are prone to mechanical failure, thus limiting their applications in practical membrane processes [11,12]. Therefore, synchronously enhancing the separation performances and mechanical strengths of hollow-fiber membranes prepared by selective swelling remains highly desired.

Nanoscale fillers are extensively used to enhance the mechanical properties of a wide range of polymeric materials [13–16]. Carbon nanotubes (CNTs) are deemed as an “ideal” reinforcement filler for their extraordinarily strong strengths, good ductility, low density, large aspects, and high surface to volume ratio [17]. However, most of the studies of CNT-doped polymeric membranes have been focused on the electrical conductivity conferred by CNTs to the membranes, while the effect of CNTs on the morphologies and mechanical properties of the membranes was rarely explored [18–20]. Theoretically, the incompatibility between CNTs and polymers allowed the membranes to achieve higher porosity, which may change the separation performances of the membranes. Specifically, Sirkar et al. [21] introduced the concept of ‘nanocorridor’ for flux increment. The modified MWCNT was incorporated into polyamide membrane and CNT-doped polymer membrane was formed by interfacial polymerization. The transport corridor between an individual MWCNT and the surrounding polymer chains provide a low-resistance pathway for solvent and water transport. Lee et al. [22] doped oxidized CNTs (0.5 wt%) into polysulfone (PSF) to prepare nanocomposite membranes via the process of nonsolvent-induced phase separation (NIPS). Herein, the increased surface porosity was mainly ascribed to the formation of enhanced pores induced by the incompatibility between CNTs and PSF, and thereby the improved water permeance. Liu et al. [23] incorporated poly(ethylene glycol)-grafted CNTs (0.6 wt%) into poly(vinylidene fluoride) (PVDF) to prepare nanocomposite membranes via NIPS. The composite membranes exhibit improved water permeance, unfortunately, at the expense of BSA retention. Besides, to prevent the agglomeration of CNTs surface functionalization to CNTs was typically necessary to introduce active groups on CNTs surfaces to enhance the repulsion between tubes. Although covalent functionalization can result in stable dispersions of CNTs, it requires harsh reaction conditions and usually comes with the cost of structure damaging such as shortening in the length of CNTs [24,25]. Therefore, enhanced mechanical properties are often not obtained for these membranes.

Interestingly, amphiphilic BCPs have been reported to be highly effective in assisting CNTs dispersing in polymer substrates without damaging the structure and physical properties of the dispersed nanotubes [26,27]. For example, poly(styrene-*b*-(isoprene-*ran*-epoxyisoprene)-*b*-styrene) has been reported to efficiently assist the dispersion of polystyrene-grafted CNTs through noncovalent functionalization [28]. Besides, Shevate et al. [29] prepared polystyrene-*b*-poly(4-vinyl pyridine) (PS-*b*-P4VP) isoporous membranes doped with 1 wt% CNTs. CNTs were dispersed homogeneously in the membrane without disturbing the pore uniformity of the membranes. However, the effect of CNTs on the mechanical properties and separation performances of membranes was unexplored. The solvophobic blocks are adsorbed to CNTs following a nonwrapping mechanism while the solvophilic blocks help the CNTs/BCPs complex to be disperse in the solvent [30]. Therefore, we anticipate that CNTs are able to reshape the thermodynamic balance between the BCPs and CNTs, thus optimizing the morphology of the CNT-doping block copolymer membranes. This will be helpful in obtaining membranes with simultaneous enhanced permeance, mechanical properties and separation properties.

CNTs has been extensively doped in polymeric membranes to enhance their mechanical properties. However, in the present work, we used the newly emerged method, selective swelling of block copolymers,

Table 1
CNTs with varied diameters and lengths.

Designation of CNTs	Diameter (nm)	Length (μm)
4-nm/10- μm CNTs	4–6	10–20
10-nm/0.5- μm CNTs	10–20	0.5–2
10-nm/10- μm CNTs	10–20	10–20
10-nm/50- μm CNTs	10–20	~50

to prepare ultrafiltration membranes and there are no previous reports on doping CNTs in membranes prepared by selective swelling. In addition to enhanced mechanical stability as observed by previous works [12], the presence of CNTs in block copolymer membranes significantly influences the swelling behaviors of block copolymers and consequently the separation performances of the resulted membranes, which has never been reported before. In this work, the CNTs are first doped into PSF-*b*-PEG substrate by melt blending with very small dosage down to 0.01 wt%. Because of the extremely low usages of CNTs in our membranes and the maturing synthesis of CNTs in large scale, such a preparation process is economically affordable and is well rewarded by the improved performances. The PSF-*b*-PEG hollow fibers doped with CNT are spun by melt extruding, and subsequently they are converted to hollow-fiber membranes by cavitating the fiber walls following the mechanism of selective swelling. It is discovered that the dosage and the aspect ratio of CNTs play a significant role in determining membrane morphologies and consequently separation performances by influencing the microphase separation and selective swelling process of the block copolymer. We demonstrate that by doping with very small amount of CNTs, the PSF-*b*-PEG ultrafiltration membranes exhibit simultaneously enhanced separation performances and mechanical strengths.

2. Experimental section

2.1. Materials

PSF-*b*-PEG with a M_n of 79.1 kDa (the weight percentage of PEG is ~21 %) was obtained from Nanjing Bangding. Multiwalled CNTs with the purity of ~95 % having varied diameters and lengths were provide by XFNANO Materials Technology Co., Ltd, and detailed information are listed in Table 1. Acetone (>99.0 %), *n*-propanol (>99.0 %), and *n*-heptane (>99.0 %) were provide by local suppliers. Bovine serum albumin (BSA, 66 kDa, >97 %) was purchased from Sigma-Aldrich. Deionized (DI) water (with a conductivity of 8–20 $\mu\text{S cm}^{-1}$) was homemade and used throughout this work.

2.2. Preparation of CNT-doping block copolymer membranes

The preparation process of CNT-doping PSF-*b*-PEG hollow-fiber membranes is shown in Fig. 1a, which mainly includes two steps: melt-spinning and selective swelling. During the melt spinning process, determined amount of CNTs and PSF-*b*-PEG were firstly added to a desktop twin-screw extruder with a heating spinneret (Xinshuo, WLG10G) to mix for 2 h. Then they were extruded to form primary hollow fibers. The extruder contains two cavities and the temperature was maintained at 180 °C for the upper cavity and 190 °C for the lower cavity. During the selective swelling process, primary hollow fibers of PSF-*b*-PEG doped with CNTs were immersed in the mixture of 20 wt% acetone and 80 wt% *n*-propanol at 65 °C for 2 h to generate interconnected pores with tens of nanometers in the walls of the membranes. Thus-treated membranes were dried at 40 °C for at least 4 h to evaporate residue solvents, producing CNT-doped hollow-fiber membranes. All other CNTs with different diameters and lengths were doped into PSF-*b*-PEG hollow-fiber membranes separately using the identical process.

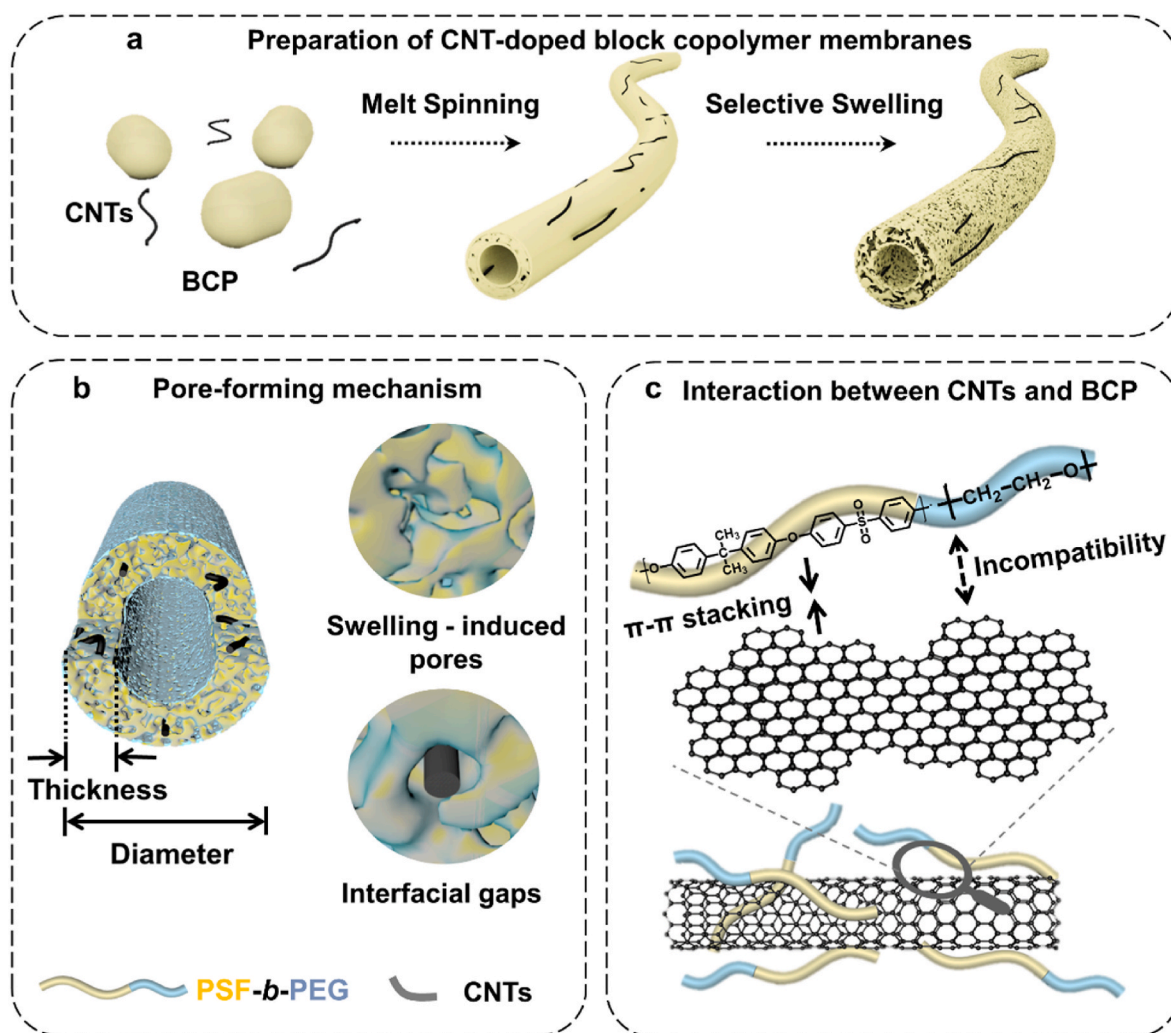


Fig. 1. Schematic illustration of (a) the preparation of CNT-doping PSF-*b*-PEG hollow-fiber membranes, and (b) the pore-forming mechanism of PSF-*b*-PEG and CNT-doping PSF-*b*-PEG (c) the interaction between CNTs and PSF-*b*-PEG.

2.3. Characterizations

The surface and cross-sectional morphologies of hollow fibers and hollow-fiber membranes were characterized using a field-emission scanning electron microscope (FE-SEM, Hitachi S4800) at the accelerating voltage of 5 kV. The cross sections of samples were prepared by fracturing in liquid nitrogen. Before imaging, all samples were sputter-coated with gold at a current of 15 μ A for 20 s to enhance the conductivity. *Image J* and *Nano Measure* were used to calculate the pore size and distribution of the membrane surface through SEM images. Nitrogen adsorption/desorption analysis was conducted by a surface area and porosity analyzer (MicrotracMRB, Belsorp-max) at 77 K. Surface areas and pore size distributions were determined from the sorption curves based on nonlocal density functional theory (NLDFT). Surface morphologies were examined by atomic force microscopy (AFM, XE-100, Park Systems) at a noncontact mode. The samples were pasted onto the silicon substrate. Transmission electron microscopy (TEM) was performed using a FEI Talos F200X G2 electron microscope at a voltage of 200 kV. The hollow-fiber membranes were implanted into epoxy resin and cured, and then microtomed by a diamond knife to obtain thin slices. The slice was transferred onto a copper grid for TEM characterizations. The PEG content on the membrane surface was characterized by X-ray photoelectron spectroscopy (XPS, Thermo Fisher K-alpha). Fourier transform infrared (FTIR) spectroscopy (Nicolet 8700 spectrometer, Thermo Fisher Scientific, USA) was utilized to probe the chemical

composition of the hollow fibers before and after doped with CNTs in the attenuated total reflection (ATR) mode. Herein, the infrared spectra within the wave number from 800 to 3500 cm^{-1} was analyzed. The CNTs and hollow-fiber membranes were secured to the silicon substrates to perform Raman spectroscopy analysis by a Raman spectrometer (HR800, Labram) with a laser wavelength of 532 nm.

2.4. Separation performances

The water permeability and rejection performance were measured by a homemade cross-flow filtration device. The membranes were pre-pressed for 10 min to obtain a stable permeance. Then, the membranes were tested for 30 min, taking samples every 5 min to calculate the average permeance. The pressure during the test was 2 bar. In the tests, the same three hollow-fiber membranes were evaluated to obtain the corresponding average value. The permeance was calculated by the following equation:

$$\text{Permeance} = \frac{V}{\Delta P \times A \times t} \quad (1)$$

where V (L) represents the total volume of water transmitted through the membrane during the test, ΔP (bar) is the operating pressure, A (m^2) is the effective area, and t (h) is the test duration.

The BSA solution (0.5 g L^{-1}) was used as the feed to evaluate the separation performance of the membranes. The concentrations of BSA in

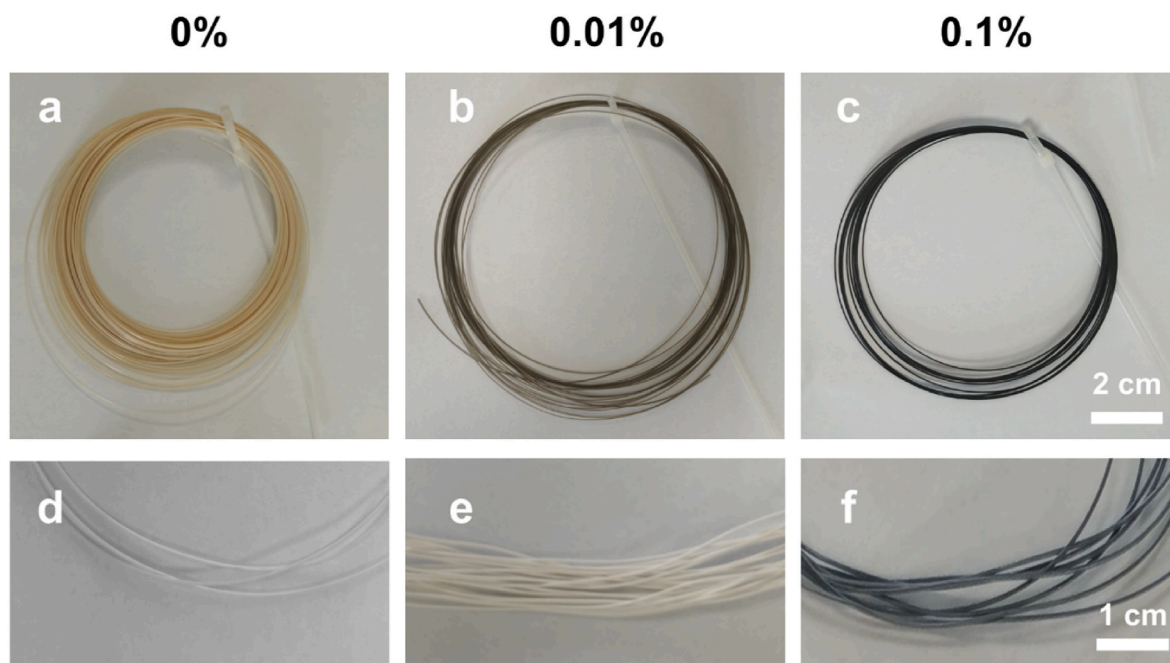


Fig. 2. Digital photographs of PSF-*b*-PEG hollow fibers (a–c) and hollow-fiber membranes (after swelling) (d–f) doped with different dosages of 4-nm/10- μ m CNTs.

the stock and cut-off solutions were measured using a UV-vis-NIR spectrophotometer (Lambda 950, PerkinElmer). The membrane rejection (R) to BSA was calculated by the following equation:

$$R(\%) = \left(1 - \frac{C_p}{C_f}\right) \times 100\% \quad (2)$$

where C_f (g L^{-1}) and C_p (g L^{-1}) are the concentrations of BSA in the stock and cut-off solutions, respectively. The concentration of the BSA solution was measured at a wavelength of 280 nm.

2.5. Mechanical properties

The tensile properties of the hollow-fiber membranes were tested by an electronic tensile testing machine (CMT6103, Shenzhen SANS) with the initial clamping distance of 100 mm at a speed of 10 mm min^{-1} . The strain at break (%) and tensile stress (MPa) were calculated by Eq. (3) and Eq. (4), respectively:

$$\text{Strain} = \frac{\Delta l}{l} \times 100\% \quad (4)$$

where Δl (mm) and l (mm) represent the change in length of the fibers during test and the initial length, respectively.

$$\text{Stress} = \frac{P}{A} \quad (3)$$

where P (N) represents the load during the test, A (mm^2) represents the cross-sectional area of the membranes.

The flexural properties of the membranes were characterized by flexural strength index. A 10-cm-length fiber was fixed vertically to the epoxy resin, and was applied a stable tensile tension (10 % tensile fracture tension of the corresponding membrane). Each fiber was reciprocating swung with a swinging amplitude at an angle of 90° until fractured or the membrane layer broken. The times of reciprocating swinging was defined as the flexural strength index of the hollow-fiber membrane.

3. Results and discussion

3.1. Dispersion of CNTs in PSF-*b*-PEG

The dispersion of CNTs in polymers is usually a problem because of the relatively strong the electrostatic forces and van der Waals' interaction between CNTs. However, amphiphilic BCPs are reported to be potential in improving the dispersion of CNTs [27,31]. In this work, CNTs and the copolymer were added in the extruder, followed by blending and self-cycling for 2 h to make sure that CNTs were sufficiently dispersed in the copolymer matrix. Then the melt was extruded through the spinneret, thus obtaining the PSF-*b*-PEG/CNTs hollow fibers. The uniform dispersion of CNTs in the PSF-*b*-PEG could be vividly observed by the homogeneous color of the hollow fibers and hollow-fiber membranes. It can be seen in Fig. 2, the hollow fibers of the neat copolymer were yellowish and turned to be white after swelling as a result of pore formation. With the doping of CNTs even at a dosage as low as 0.01 wt%, the hollow fibers took a grey color which are uniform throughout the entire fibers. At a CNTs dosage of 0.1 wt%, the fibers took a uniform black color. After swelling, the fibers turned to be greyish and the color became darker with higher CNTs dosages but still remained uniform. From Fig. S2, we can scarcely observe CNTs in the polymer matrix due to the extremely low dosages of CNT. However, the CNTs were isolated, and no agglomeration was observed, which can be ascribed to the favorable interaction between CNTs and the PSF phase of the BCP substrate [32].

In the present work, the block copolymer, PSF-*b*-PEG was utilized as the polymer matrix to host CNTs. The PSF as the majority block in the copolymer forms the continuous phase, and it carries many benzene rings which have π - π interaction with the phenyl structures on sidewalls of CNTs, thus facilitating the dispersion of CNTs in the PSF-*b*-PEG and preventing the aggregation of CNTs. However, the PEG block forming the dispersed phase in the copolymer is highly hydrophilic, and it is expected that PEG phases are highly incompatible to CNTs which are strongly hydrophobic [33]. As a result, CNTs tend to avoid contacting the PEG microdomains in the PSF matrix. However, because of the rigid nature of CNTs and the lengths of CNTs (in the scale of micrometers) much larger than the size of the PEG microdomains (in the scale of several tens of nanometers), CNTs have to contact and even penetrate

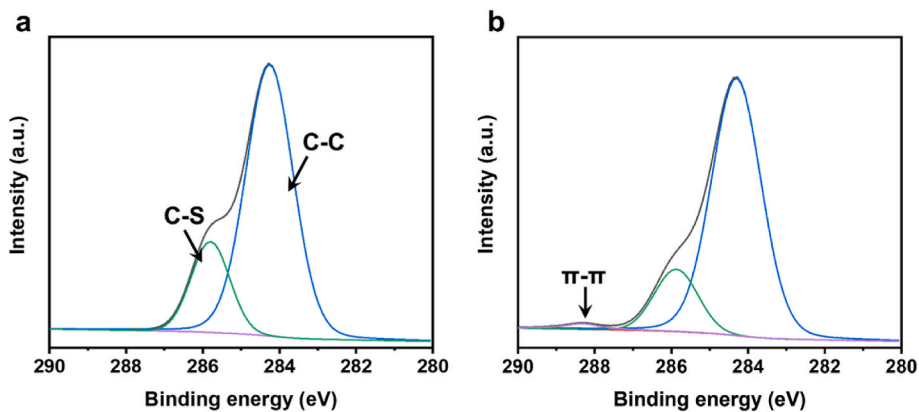


Fig. 3. C 1s spectrum of (a) PSF-*b*-PEG membranes and (b) CNT-doped PSF-*b*-PEG membranes measured by XPS.

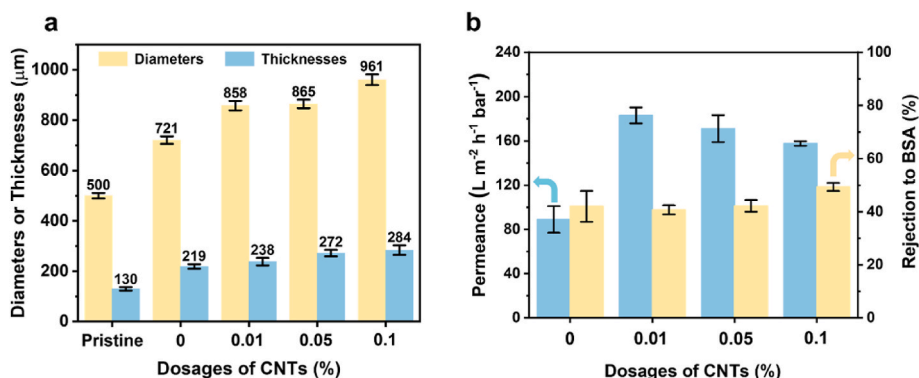


Fig. 4. (a) Outer diameters and thicknesses of the pristine hollow fibers and hollow-fiber membranes with different 4-nm/10-μm CNT dosages. (b) Water permeance and rejection properties of hollow-fiber membranes doped with different dosages of 4-nm/10-μm CNTs.

the PEG microdomains with interfacial gaps forming between CNTs and PEG domains as a response to the incompatibility between them (Fig. 1c). Unless there is an extraordinarily high density of surface functionalized groups (on the outside of the MWCNTs) which interact actively with the matrix polymer, such gaps will exist [21]. Moreover, the shear force at high rotating speeds during blending and extruding also contributed to overcoming the strong interactions between CNTs, thus unwrapping the entangled CNT agglomerates [34]. Therefore, the presence of CNTs in block copolymer might affect the thermodynamic balance of the polymer components, and thus may regulate the phase separation in BCPs [35].

Wrapping of CNTs may be driven by chemical interactions between the π -system of the CNT and the functional groups comprising the polymers: electrostatic interactions, π -stacking, and hydrogen bonding were found to dominate in different systems [30]. X-ray photoelectron spectroscopy (XPS) analysis evidenced the interaction between CNTs and PSF (Fig. 3). The narrow scan spectra of C 1s reveal C-C at 284.8 eV and C-S at 286.2 eV. Importantly, the new peak at a higher binding energy of 288.1 eV indicated the existence of π - π interaction [36]. In the present work, the interaction between CNTs and BCPs is predominantly to be π - π interaction as implied by the XPS characterization (Fig. 3). We also performed Raman and IR characterizations on the hollow-fiber membranes with various CNTs dosages, and observed neither any new peaks other than those originated from the CNTs and copolymers nor position change of their characteristic peaks (Fig. S3). This implies that both melt spinning and selective swelling were physical processes and no chemical reactions took place during the fabrication of the CNTs-doped hollow-fiber membranes. Because of the uniform dispersion of CNTs in the copolymer, the hollow fibers maintained a smooth surface after doping with CNTs and no cracks or defects appear.

3.2. Effect of CNT dosages

Before swelling treatment, the neat and the CNTs-doped hollow fibers exhibit similar outer diameter and wall thickness (Fig. 4a), which were ~ 500 μm and ~ 130 μm , respectively. After selective swelling, the fiber parameters of the neat membrane were expanded to ~ 721 μm and 219 μm , respectively as a result of the formation of pores induced by selective swelling [12]. After doping with 0.01 wt% CNTs, the fiber parameters were expanded to 858 μm and 238 μm , respectively. With the CNTs dosage further increased to 0.05 and 0.1 wt%, the wall thicknesses raised to 272 and 284 μm , respectively. It is clear that hollow-fiber membranes with higher CNTs dosages experienced larger increment in wall thickness and consequently larger pore volumes. The increased pore volumes for the CNT-doped membranes should be ascribed to interfacial gaps caused by the incompatibility between CNTs and PEG microdomains. That is, in the CNT-doped membranes there are two sets of pores: one is caused by selective swelling, and the other is caused by the incompatibility between CNTs and PEG microdomains (Fig. 1b).

We used SEM to examine the surface and the cross-sectional morphology of the CNT-doped membranes. As shown in Fig. S4, they all exhibited a highly porous structure but the pore size cannot be quantitatively analyzed based on the SEM images as the pores were three-dimensionally interconnected. Alternatively, nitrogen adsorption characterizations were performed to investigate the porous nature of the membranes doped with different dosages of CNTs. The neat hollow-fiber membrane without CNTs doping exhibited a BET surface area of 32.5 $\text{m}^2 \text{g}^{-1}$, which was increased to 44.7 $\text{m}^2 \text{g}^{-1}$ after being doped with 0.01 wt% CNTs. The enlarged surface areas should be caused by the incompatibility between CNTs and PEG microdomains. The specific

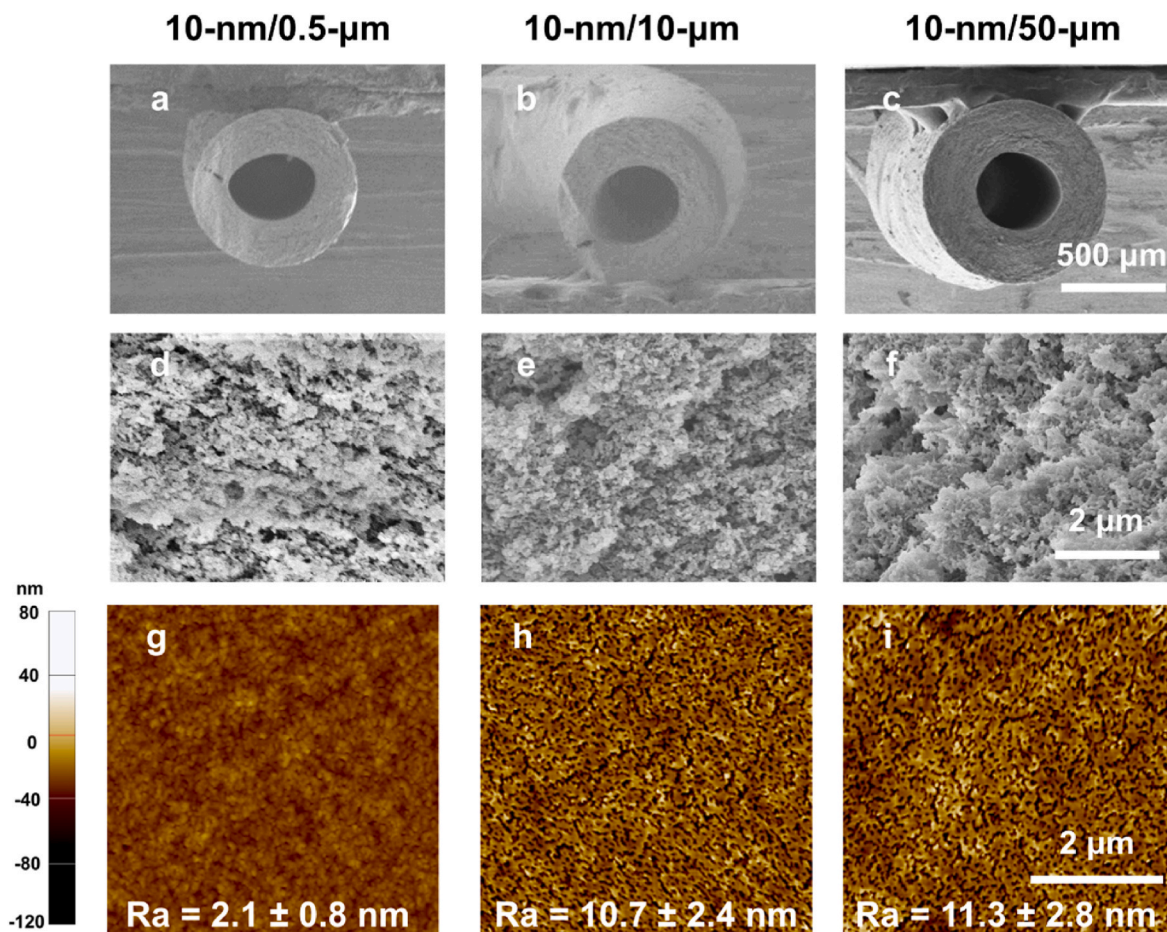


Fig. 5. (a–c) Cross-sectional pictures, (d–f) cross-sectional SEM images of the CNT-enhanced PSF-*b*-PEG membranes with CNTs of various aspects. (g–i) AFM images of the CNT-doping PSF-*b*-PEG membranes with CNTs of various aspects. The roughness parameters of the membranes were presented in the pictures.

surface area decreased to 40.7 and 39.6 m² g⁻¹ when the CNT dosage was increased to 0.05 wt% and 0.1 wt% CNTs, respectively, but were still higher than that of the neat membrane. CNTs doping influences the pore formation process of PSF-*b*-PEG in two opposite ways. On one hand, CNTs weaken the plastic deformation of the PSF continuous phase and consequently refrain the pore formation of the copolymer to some extent by selective swelling because of the π - π interaction between CNTs and PSF chains, and as a result selective swelling will produce smaller pores on membrane surfaces. On the other hand, the incompatibility between CNTs and PEG results in interfacial gaps, thus producing more pores. These two competing effects eventually determine the porous structure of the membranes.

It has been reported that the hydrophilic blocks will preferably migrate to the pore wall and membrane surface when amphiphilic block copolymers, like PSF-*b*-PEG, are swelling treated in a polar solvent selective to the hydrophilic blocks [37]. This surface enrichment of PEG blocks during the selective swelling of PSF-*b*-PEG is also influenced by CNTs doping. XPS was utilized to analyze the surface enrichment of PEG blocks on the membranes. O 1s was probed within the scope of 525.08–545.08 eV by narrow scan. The peak at the binding energy of 532.3 eV (C–O–C) was assigned to the O 1s in PEG blocks, and the peaks at 533.1 eV (Ph–O–Ph) and 531.6 eV (S=O) were derived from O 1s in PSF blocks. The ratio of the area of the C–O–C peak to the area of the O 1s peak is an indicator of the surface dosages of PEG enriched onto the membrane surface. As presented in Fig. S6, the PEG content on the surface of the neat membrane was ~34 %, which was increased to 37, 40, and 43 % for the membrane doped with 0.01, 0.05, and 0.1 wt% CNTs, respectively. More PEG chains enriched onto membrane surface

with higher CNTs dosages is also caused by the incompatibility of CNTs and PEG blocks. Higher CNTs dosages means more PEG chains unfavorably interact with CNTs, producing more interfacial gaps. Consequently, more PEG chains were mitigated onto the membrane surface.

The permeances of hollow-fiber membranes doped with different CNTs dosages were tested and shown in Fig. 4b. The water permeance of the neat membrane was 89.0 L m⁻² h⁻¹ bar⁻¹. For membranes with 0.01, 0.05 and 0.1 wt% doped CNTs, the water permeance were increased to 183.0, 171.1 and 157.6 L m⁻² h⁻¹ bar⁻¹, respectively. The water permeance of CNTs-doped membranes were all higher than that of the neat membrane. This was mainly ascribed to the additional pores provided by the interfacial gaps between CNTs and PEG [21]. Moreover, the enrichment of PEG on the membrane surface also contributes the increase in water permeance. We note that the change tendency of permeance with CNTs dosages was in accordance with the change of surface areas and pore sizes of the membranes doped with various CNTs dosages (Fig. S5i–l). According to our previous work, the rejection mechanism of PSF-*b*-PEG hollow fiber membrane towards BSA is mainly functioned by the size discrimination effect [10]. The rejection to BSA (molecular size: 14.1 nm × 4.2 nm × 4.2 nm) of these hollow-fiber membranes were also measured. All these membranes showed similar rejection properties (40 %–50 %) regardless of the CNTs dosages. That is, CNTs doping evidently increases the water permeance of the membranes at no expense of rejection, and this is because another set of pores (interfacial gaps between CNTs and PEG microdomains) smaller than the pores induced by selective swelling allow more water to pass but reject BSA.

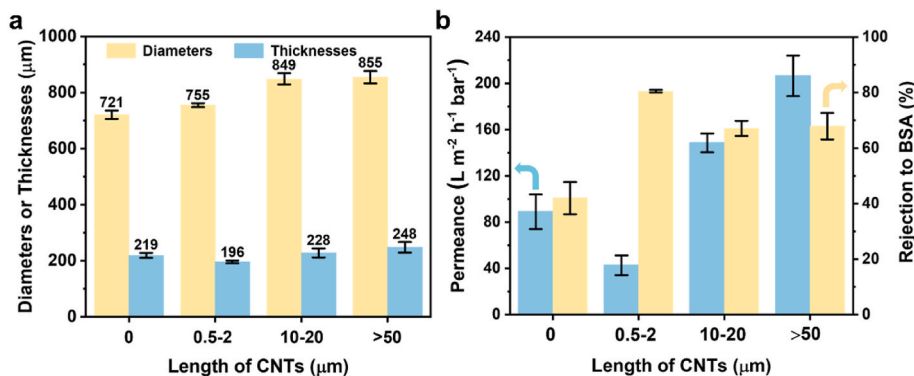


Fig. 6. (a) Outer diameters and thicknesses and (b) water permeance and separation properties of the neat membranes and the membrane doped with 0.01 wt% 10-nm-diameter CNTs having the tube lengths of 0.5, 10, and 50 μm , respectively.

3.3. Effect of CNTs aspects

Nanofillers with various aspects showed different interfacial stability and mobility in polymer melts [38,39]. We prepared PSF-*b*-PEG hollow-fiber membranes doped with 0.01 wt% 10-nm-diameter CNTs with the tube lengths of 0.5, 10, and 50 μm , respectively. Interestingly, the morphologies and the performance of these membranes varied greatly with the tube lengths. As is shown in Fig. 5a–c, the wall thickness of membrane doped with 0.5-, 10-, and 50- μm -length CNTs was 196, 228, and 248 μm , respectively. Furthermore, the BET surface areas and average pore sizes of these three membranes were 30.7, 41.4 and 67.5 $\text{m}^2 \text{g}^{-1}$, and 25.4, 38.1, and 46.1 nm (Fig. S7), respectively. We then examined the morphology of these membranes. Cross-sectional SEM observation confirms that the three membranes all show a highly porous nature (Fig. 5d–f). AFM examinations reveal that pores were also present on the surface of all the three membranes, and membranes doped with shorter CNTs showed smaller pores (Fig. 5g–i). The membrane doped with 0.5- μm -length CNTs exhibited a relatively dense and smooth surface with a roughness of 2.1 nm, and the membrane doped with 10-, and 50- μm -length CNTs exhibited higher roughness of 10.7, and 11.3 nm, respectively. All these characterizations consistently indicate that longer CNTs in the membranes led to bigger pores and larger porosities. It has been reported that the length of CNTs would affect their movement and distribution in the polymer matrix [40]. In the melt blending process, shorter CNTs should move faster and migrate more completely into the PSF phase, thus minimizing the thermodynamic unfavorable contact with the PEG microdomains. Consequently, less interfacial gaps between CNTs and PEG are produced. In addition, shorter CNTs have more chance to be distributed in the PSF continuous phase. That is, the plastic deformation of the PSF phase will be refrained to a higher degree, and as a result selective swelling will produce smaller pores. The two effects take place simultaneously, leading to lower porosities in the membrane doped with shorter CNTs.

We note that the CNT length strongly influences the swelling and pore formation of PSF-*b*-PEG membranes. The membrane doped with 0.5- μm -length CNTs exhibited thinner thickness (196 μm vs 219 μm) and smaller pores (5.9 nm vs 18.2 nm) (Fig. S7g–i) than the neat membrane without CNTs doping. This is because the shortest 0.5- μm -length CNTs restrict the selective swelling-induced pore generation of the PSF-*b*-PEG. For longer CNTs with length of 10 and 50 μm , their doping in the copolymer will facilitate the swelling and pore formation (9.6 nm and 13.9 nm) of the copolymer.

The permeance and the separation properties of these membranes were shown in Fig. 6b. When the length of CNT was 0.5, 10 and 50 μm , the membrane permeance were 42.7, 148.5, and 206.4 $\text{L m}^{-2} \text{h}^{-1} \text{bar}^{-1}$, respectively. This can be readily explained by the rising porosities with the increased CNTs length. In addition, their rejection to BSA were 80.5 %, 67.1 % and 67.9 %, respectively. It is interesting that all three

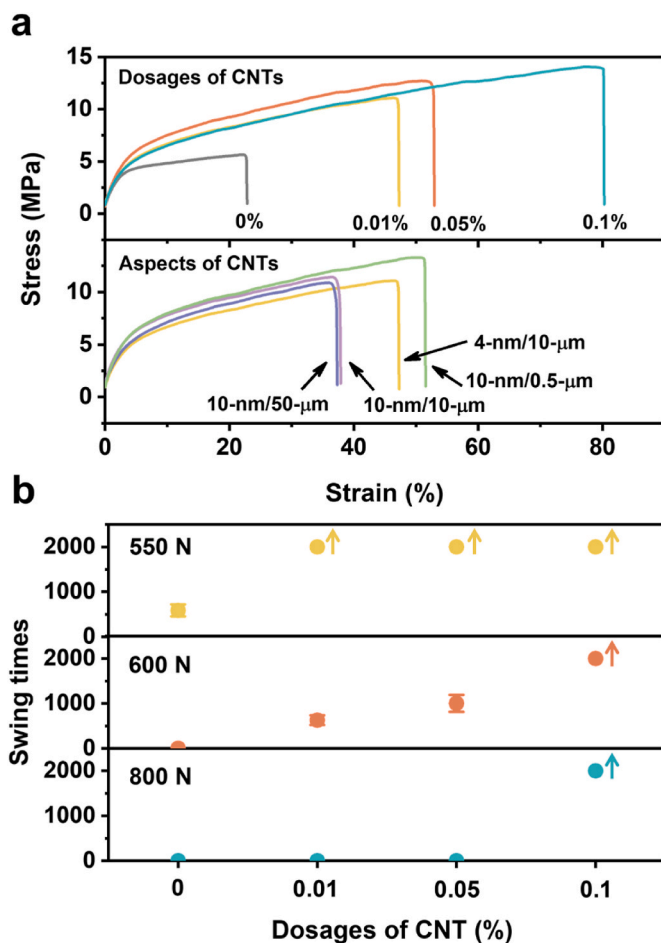


Fig. 7. (a) Stress-strain curves of PSF-*b*-PEG hollow-fiber membranes doped with various dosages and aspects of CNTs. (b) The flexural properties of PSF-*b*-PEG hollow-fiber membranes doped with 4-nm/10- μm CNTs with various dosages. The arrows in (b) mean that swing times were larger than 2000 times.

membranes doping with different length of CNTs show enhanced rejection performance compared with the PSF-*b*-PEG membrane, this may be ascribed to the narrowed surface pore sizes mentioned above. As we mentioned, the rejection mechanism of PSF-*b*-PEG hollow-fiber membrane towards BSA is mainly functioned by the size discrimination effect. The average size of pores on membrane surface were smaller than the long axis length of BSA (14.1 nm), which must be the main reason contributing to the high rejection to BSA. We note that the best

Table 2
Properties of CNT-doping PSF-*b*-PEG hollow-fiber membranes.

Samples	Dosages of CNTs (wt%)	Diameters & lengths of CNTs (nm/ μ m)	Permeance(LMHB)	Rejection to BSA (%)	Stress (MPa)	Strain (%)
1	0	0	89 \pm 12	42 \pm 5.8	5.7	23
2	0.01	4/10	183 \pm 7.2	40.7 \pm 1.7	9.7	48
3	0.05	4/10	171.1 \pm 12.2	42.2 \pm 2.2	12.6	53
4	0.1	4/10	157.6 \pm 2.1	49.3 \pm 1.5	14.0	80
5	0.01	10/0.5	42.7 \pm 8.5	80.5 \pm 0.5	12.7	51.7
6	0.01	10/10	148.5 \pm 8.1	67.1 \pm 2.7	10.2	38.3
7	0.01	10/50	206.4 \pm 17.5	67.9 \pm 4.8	9.5	38.0

performance (206.4 L m⁻² h⁻¹ bar⁻¹, and 67.9 %) was achieved when doping 0.01 wt% of CNTs with the diameter of \sim 10 nm and the length of \sim 50 μ m. This is remarkable as the permeance is three times higher than that of the neat PSF-*b*-PEG membrane while the rejection is 1.6 times higher especially when we consider that only a very small dosage down to 0.01 wt% of CNTs was doped into the block copolymer. We examined the existence of CNTs in water passing through the CNTs-doped membrane, and we did not find any detectable CNTs in this water (Fig. S8). Therefore, we conclude that block copolymer chains heavily interwounded with CNTs, preventing CNTs leakage, and there is no need to concern about environmental impacts related to the CNTs leakage. Compared to other UF membranes prepared by melt processing, our CNT-doped PSF-*b*-PEG membranes exhibit higher flux and better mechanical robustness (Table S1). Moreover, our membranes are also distinctive in two aspects. The first is their inherent hydrophilic surfaces as a result of the enrichment of PEG blocks to the membrane surfaces during selective swelling. The second is the nondestructive nature of pore-forming process which does not require removing any components from the membrane-forming materials and produces no wastes during pore formation. In contrast, most other melt-processed UF membranes are hydrophobic in nature, and their pores are produced by removing pre-mixed additives. We note that our membranes need further optimization to improve their rejections for specific applications.

3.4. Enhancement of mechanical properties

Tensile tests of hollow-fiber membranes doped with different dosages of CNTs were performed. As shown in Fig. 7a, the neat membrane without CNTs doping displayed a tensile stress of 5.7 MPa and a strain at break of 23 %. After doping with 0.01 and 0.1 wt% 4-nm/10- μ m CNTs, the tensile stress was increased to 9.7 and 14.0 MPa while the strain at break increased to 48 and 80 %, respectively. The increasement of both tensile stress and the strain at break should owe to the mechanical enhancing effect of CNTs to the polymeric matrix [41]. We then investigated the effect of CNTs lengths on the tensile properties of the hollow-fiber membranes. Tensile stress of membranes doped with 0.01 wt% 10-nm-diameter CNTs with the length of \sim 0.5, 10, 50 μ m were 12.7, 10.2 and 9.5 MPa, and their strain at break were 51.7, 38.3 and 38.0 %, respectively. Clearly, shorter CNTs enhance the mechanical properties of the membrane to a higher degree. This is because such short CNTs are preferentially concentrated in the PSF continuous phase, and the π - π interaction between CNTs and PSF are stronger. As a result, the membrane is significantly enhanced.

Besides, the flexural properties of these membranes were characterized by measuring the swing times before the fiber fracture. As shown in Fig. 7b, the neat membrane fractured after \sim 586 times of swinging under the force of 550 N, and it cannot tolerate the swing force of 600 N at all as it was broken immediately when such a force was applied. Interestingly, when doped with only 0.01 wt% of 4-nm/10- μ m CNTs, the hollow-fiber membrane did not break even after swing for 2000 times at an applied force of 550 N. With the increasing CNTs dosages, the flexural properties of the membranes were continuously enhanced. The membrane with 0.05 and 0.1 wt% CNTs cannot survive an applied force of 800 N. However, the membrane doped with 0.1 wt% 4-nm/10- μ m CNTs maintained intact and unbroken even after swinging at 800 N for >2000

times. Therefore, both the tensile properties and the flexural properties of the membranes were significantly increased after CNTs doping and higher dosages of CNTs led to better mechanical properties. Although we are still optimizing the preparation parameters of the CNT-doped PSF-*b*-PEG membranes to maximize their performances (Table 2), the membranes are expected to exhibit good stability, durability and fouling resistance because of their excellent mechanical strength and the PEG-enriched membrane surfaces which are highly tolerant to adsorption and fouling.

4. Conclusions

In this work, CNT-doping PSF-*b*-PEG hollow-fiber membranes are fabricated by melt blending and melt spinning followed by selective swelling. The CNT-doping PSF-*b*-PEG hollow-fiber membranes contains swelling-induced pores and interfacial gaps. With the dosages of CNTs increased, the selective swelling was limited, but the interfacial gaps between CNTs and BCPs increased. The membranes showed higher surface areas and smaller pores, which were responsible for the high water permeance without sacrificing BSA rejection. Besides, the morphology and properties of the membrane can also be adjusted by tuning the CNT aspect ratio. Short and thin CNTs tend to have a stronger π - π interaction between CNTs and PSF, thus producing smaller pores and decreasing permeance by refraining selective swelling to a larger degree. On the contrary, long CNTs contribute to the improvement of membrane permeance and separation performance. Otherwise, thanks to the strong mechanical strength of CNTs, the CNT-doping PSF-*b*-PEG hollow-fiber membranes achieve enhanced tension resistance and flexural properties. This work demonstrates the great potential of CNT doping in upgrading both permeability and separation performances as well as the mechanical stability of BCP hollow-fiber membranes.

CRedit authorship contribution statement

Xiang Ying: Writing – original draft, Investigation, Data curation. **Shoutian Qiu:** Writing – review & editing, Validation, Funding acquisition. **Zhuo Li:** Methodology, Investigation. **Lei Wang:** Investigation. **Kang Zhou:** Investigation. **Xiangyue Ye:** Investigation. **Jiemei Zhou:** Validation, Methodology. **Sheng Cui:** Validation, Methodology. **Yong Wang:** Writing – review & editing, Supervision, Funding acquisition, Conceptualization.

Declaration of competing interest

The authors declare that they have no known competing financial interests or personal relationships that could have appeared to influence the work reported in this paper.

Acknowledgments

This work was financially supported by the National Key Research and Development Program of China (2024YFE0112300), and the National Natural Science Foundation of China (22438005, 22108117).

Appendix A. Supplementary data

Supplementary data to this article can be found online at <https://doi.org/10.1016/j.memsci.2025.124019>.

Data availability

Data will be made available on request.

References

- [1] L. Guo, K. Ntetsikas, G. Zapsas, R. Thankamony, Z. Lai, N. Hadjichristidis, Highly efficient production of nanoporous block copolymers with arbitrary structural characteristics for advanced membranes, *Angew. Chem. Int. Ed.* 62 (2023) e202212400.
- [2] L. Guo, Y. Wang, M. Steinhart, Porous block copolymer separation membranes for 21st century sanitation and hygiene, *Chem. Soc. Rev.* 50 (2021) 6333–6348.
- [3] S. Qiu, Z. Li, X. Ye, X. Ying, J. Zhou, Y. Wang, Selective swelling of polystyrene (PS)/Poly(dimethylsiloxane) (PDMS) block copolymers in alkanes, *Macromolecules* 56 (2022) 215–225.
- [4] D. Ma, X. Ye, Z. Li, J. Zhou, D. Zhong, C. Zhang, S. Xiong, J. Xia, Y. Wang, A facile process to prepare fouling-resistant ultrafiltration membranes: spray coating of water-containing block copolymer solutions on macroporous substrates, *Sep. Purif. Technol.* 259 (2021) 118100.
- [5] D. Zhong, Z. Wang, J. Zhou, Y. Wang, Additive-free preparation of hemodialysis membranes from block copolymers of polysulfone and polyethylene glycol, *J. Membr. Sci.* 618 (2021) 118690.
- [6] Z. Li, S. Qiu, X. Ying, F. Zhang, X. Xu, Z. Cui, Y. Wang, Nanoporous thin films of hydrophobic block copolymers enabled by selective swelling for membrane distillation, *J. Membr. Sci.* 679 (2023) 121710.
- [7] H. Yang, X. Shi, S. Chu, Z. Shao, Y. Wang, Design of block-copolymer nanoporous membranes for robust and safer lithium-ion battery separators, *Adv. Sci.* 8 (2021) 2003096.
- [8] Y. Dou, X. Dong, Y. Ma, P. Ge, C. Li, A. Zhu, Q. Liu, Q. Zhang, Hollow fiber ultrafiltration membranes of poly(biphenyl-trifluoroacetone), *J. Membr. Sci.* 659 (2022) 120779.
- [9] M. Khayet, M. Essalhi, M.R. Qtaishat, T. Matsuura, Robust surface modified polyetherimide hollow fiber membrane for long-term desalination by membrane distillation, *Desalination* 466 (2019) 107–117.
- [10] X. Ying, S. Qiu, X. Ye, Z. Li, J. Zhou, Y. Wang, Elution-free hollow-fiber membranes of block copolymers for hemodialysis balancing protein retaining and toxin clearance, *J. Membr. Sci.* 695 (2024) 122457.
- [11] D. Zhong, S. Qiu, J. Zhou, D. Ma, Y. Wang, Selective swelling of stretched block copolymer hollow fibers for upgraded membrane performance, *ACS Appl. Polym. Mater.* 4 (2022) 7989–7997.
- [12] D. Zhong, J. Zhou, Y. Wang, Hollow-fiber membranes of block copolymers by melt spinning and selective swelling, *J. Membr. Sci.* 632 (2021) 119374.
- [13] I. Pastoriza-Santos, C. Kinnear, J. Pérez-Juste, P. Mulvaney, L.M. Liz-Marzán, Plasmonic polymer nanocomposites, *Nat. Rev. Mater.* 3 (2018) 375–391.
- [14] J. Zhang, P.J. Santos, P.A. Gabrys, S. Lee, C. Liu, R.J. Macfarlane, Self-assembling nanocomposite tectons, *J. Am. Chem. Soc.* 138 (2016) 16228–16231.
- [15] H. Riazi, S.K. Nemani, M.C. Grady, B. Anasori, M. Soroush, Ti3C2MXene–polymer nanocomposites and their applications, *J. Mater. Chem. A* 9 (2021) 8051–8098.
- [16] J. Xiong, Y. Cao, H. Zhao, J. Chen, X. Cai, X. Li, Y. Liu, H. Xiao, J. Ge, Cooperative antibacterial enzyme-Ag-polymer nanocomposites, *ACS Nano* 16 (2022) 19013–19024.
- [17] A. Hirsch, Functionalization of single-walled carbon nanotubes, *Angew. Chem. Int. Ed.* 41 (2002) 1853–1859.
- [18] C.C. Hung, Y.C. Chiu, H.C. Wu, C. Lu, C. Bouilhac, I. Otsuka, S. Halila, R. Borsali, S. H. Tung, W.C. Chen, Conception of stretchable resistive memory devices based on nanostructure-controlled carbohydrate-block-polyisoprene block copolymers, *Adv. Funct. Mater.* 27 (2017) 1606161.
- [19] L. Liu, Y. Xu, K. Wang, K. Li, L. Xu, J. Wang, J. Wang, Fabrication of a novel conductive ultrafiltration membrane and its application for electrochemical removal of hexavalent chromium, *J. Membr. Sci.* 584 (2019) 191–201.
- [20] Y. Li, Z. Pei, D. Luan, X.W. Lou, Superhydrophobic and conductive wire membrane for enhanced CO₂ electroreduction to multicarbon products, *Angew. Chem. Int. Ed.* 62 (2023) e202302128.
- [21] S. Roy, S.A. Ntım, S. Mitra, K.K. Sirkar, Facile fabrication of superior nanofiltration membranes from interfacially polymerized CNT-polymer composites, *J. Membr. Sci.* 375 (2011) 81–87.
- [22] T.H. Lee, M.Y. Lee, H.D. Lee, J.S. Roh, H.W. Kim, H.B. Park, Highly porous carbon nanotube/polysulfone nanocomposite supports for high-flux polyamide reverse osmosis membranes, *J. Membr. Sci.* 539 (2017) 441–450.
- [23] C. Liu, W. Wang, Y. Li, F. Cui, C. Xie, L. Zhu, B. Shan, PMWCNT/PVDF ultrafiltration membranes with enhanced antifouling properties intensified by electric field for efficient blood purification, *J. Membr. Sci.* 576 (2019) 48–58.
- [24] L.-P. Yang, C.-Y. Pan, A non-covalent method to functionalize multi-walled carbon nanotubes using six-armed star poly(L-lactic acid) with a triphenylene core, *Macromol. Chem. Phys.* 209 (2008) 783–793.
- [25] V.D. Punetha, S. Rana, H.J. Yoo, A. Chaurasia, J.T. McLeskey, M.S. Ramasamy, N. G. Sahoo, J.W. Cho, Functionalization of carbon nanomaterials for advanced polymer nanocomposites: a comparison study between CNT and graphene, *Prog. Polym. Sci.* 67 (2017) 1–47.
- [26] X. Zhang, P. Dang, B. Deng, X. Xia, K. Wang, Y. Li, T. Xia, Controlled crystallization of diblock copolymers on carbon materials: effect of block length, *Appl. Surf. Sci.* 583 (2022) 152487.
- [27] D. Ma, H. Li, Z. Meng, C. Zhang, J. Zhou, J. Xia, Y. Wang, Absolute and fast removal of viruses and bacteria from water by spraying-assembled carbon-nanotube membranes, *Environ. Sci. Technol.* 55 (2021) 15206–15214.
- [28] H. Garate, M. Bianchi, L.I. Pietrasanta, S. Goyanes, N.B. D'Accorso, High-energy dissipation performance in epoxy coatings by the synergistic effect of carbon nanotube/block copolymer conjugates, *ACS Appl. Mater. Interfaces* 9 (2016) 930–943.
- [29] R. Shevate, M.A. Haque, F.H. Akhtar, L.F. Villalobos, T. Wu, K.V. Peinemann, Embedding 1D conducting channels into 3D isoporous polymer films for high-performance humidity sensing, *Angew. Chem. Int. Ed.* 57 (2018) 11218–11222.
- [30] R.S.-C. Einat Nativ-Roth, Céline Bounioux, Marc Florent, Dongsheng Zhang, Igal Szeifer, Rachel Yerushalmi-Rozen, Physical adsorption of block copolymers to swnt and mwnt: a nonwrapping mechanism, *Macromolecules* 40 (2007) 3676–3685.
- [31] Q. Lan, N. Yan, H. Yang, Y. Wang, Nanocomposite block copolymer membranes with enhanced permeance and robustness by carbon nanotube doping, *Compos. Commun.* 29 (2022) 101025.
- [32] R.J. Chen, Y. Zhang, D. Wang, H. Dai, Noncovalent sidewall functionalization of single-walled carbon nanotubes for protein immobilization, *J. Am. Chem. Soc.* 123 (2001) 3838–3839.
- [33] A. Sari, A. Bicer, F.A. Al-Sulaiman, A. Karaipekli, V.V. Tyagi, Diatomite/CNTs/PEG composite PCMs with shape-stabilized and improved thermal conductivity: preparation and thermal energy storage properties, *Energy Build.* 164 (2018) 166–175.
- [34] G. Sui, D. Liu, Y. Liu, W. Ji, Q. Zhang, Q. Fu, The dispersion of CNT in TPU matrix with different preparation methods: solution mixing vs melt mixing, *Polymer* 182 (2019) 121838.
- [35] Y.S. Lipatov, Phase separation in filled polymer blends, *J. Macromol. Sci., Part B: Phys.* 45 (2011) 871–888.
- [36] K. Mi, S. Xiong, Y. Lu, Y. Wang, Precise fabrication of robust conjugated microporous polymer membranes via oxidative molecular layer deposition for efficient organic solvent nanofiltration, *Chem. Mater.* 36 (2024) 7069–7078.
- [37] Z. Wang, R. Liu, H. Yang, Y. Wang, Nanoporous polysulfones with in situ PEGylated surfaces by a simple swelling strategy using paired solvents, *Chem. Commun.* 53 (2017) 9105–9108.
- [38] U. Staudinger, A. Janke, C. Steinbach, U. Reuter, M. Ganß, O. Voigt, Influence of CNT length on dispersion, localization, and electrical percolation in a styrene-butadiene-based star block copolymer, *Polymers* 14 (2022) 2715.
- [39] X.-d. Qi, J.-h. Yang, N. Zhang, T. Huang, Z.-w. Zhou, I. Kühnert, P. Pötschke, Y. Wang, Selective localization of carbon nanotubes and its effect on the structure and properties of polymer blends, *Prog. Polym. Sci.* 123 (2021) 101471.
- [40] A. Gödel, A. Marmor, G.R. Kasaliwal, P. Pötschke, G. Heinrich, Shape-dependent localization of carbon nanotubes and carbon black in an immiscible polymer blend during melt mixing, *Macromolecules* 44 (2011) 6094–6102.
- [41] C. Tian, J. Ning, Y. Yang, F. Zeng, L. Huang, Q. Liu, J. Lv, F. Zhao, W. Kong, X. Cai, Super tough and stable solid–solid phase change material based on π - π stacking, *Chem. Eng. J.* 429 (2022) 132447.